QUICK DAMAGE DETECTION OF URBAN AREAS USING DIGITAL AIRBORNE IMAGES

Fumio Yamazaki[1], Daisuke Suzuki[2], and Yoshihisa Maruyama[3]

1) Professor, Graduate School of Engineering, Chiba University, Japan.
2) Graduate Student, Graduate School of Engineering, Chiba University, Japan.
3) Assistant Professor, Graduate School of Engineering, Chiba University, Japan.

yamazaki@tu.chiba-u.ac.jp, daisuke.s.9-18@graduate.chiba-u.jp, ymaruyam@tu.chiba-u.ac.jp

Abstract: Remote sensing technology is effective to grasp the damage distributions from various natural disasters, such as earthquakes, tsunamis and volcanic eruptions. After the 2007 Off-Mid-Niigata, Japan earthquake, aerial images were taken in the stricken area by several air survey companies in Japan. Airborne remote sensing is more suitable to collect detailed damage distribution because it provides higher resolution images than satellite remote sensing does. The post-event image taken by a digital aerial camera (DMC) is employed in this study to detect building damages. Since visual damage inspection takes time to perform for the whole areas that are subjected to severe ground motion, an object-based technique is proposed to extract debris from buildings. The proposed method is expected to contribute for the damage assessment at an early stage after the occurrence of an earthquake.

1. INTRODUCTION

Aerial photography has been used widely for aerial surveying and photogrammetry. Because of its very high spatial resolution, aerial photographs were employed to detect damages due to earthquakes (e.g., Ogawa and Yamazaki, 2000). Digital aerial cameras, recently developed and introduced for aerial photography, have much higher radiometric resolution than traditional film (analog) aerial cameras do. Thus, even though the spatial resolution is almost the same level, e.g. 0.1 m, a digital aerial camera can capture much clearer images of the earth surface than an analog camera does.

Another important feature of digital aerial cameras is that they have a near infrared (NIR) band as well as RGB visible bands. Using the NIR band, detection of vegetation becomes quite easy. Through the pan-sharpening procedure, very-high resolution pseudo-color images can be obtained by combining these 4 multi-spectral bands and the panchromatic band. Note that the spatial resolution of high-resolution satellites currently available is 0.6 m (QuickBird) at the maximum, and thus the digital aerial images can be used for extraction of detailed damages of buildings and infrastructures (Mitomi et al., 2002; Maruyama et al., 2006).

This paper highlights the capability of digital aerial images in detecting various damages due to earthquakes. In the recent earthquakes in Japan, such as the 2004 Mid-Niigata, the 2007 Noto Peninsula, and the 2007 Off-Mid-Niigata earthquakes, the affected areas were captured by digital aerial cameras as well as by film aerial cameras and high-resolution satellites. Especially for the 2007 Off-Mid-Niigata earthquake, digital aerial cameras captured the affected area both before and after the event. Pixel-based and object-based image processing techniques are applied to those digital images, and their accuracy to extract building damage is discussed.

2. DIGITAL AERIAL IMAGES OF KASHIWAZAKI CITY

The central part of Niigata Prefecture, Japan was hit by a strong M_{JMA}=6.8 earthquake on July 16, 2007. A total 1,330 houses were collapsed or severely damaged and 15 people were killed in Niigata Prefecture. Kashiwazaki City was most severely affected in the prefecture with 1,120 collapsed or severely damaged houses and 14 deaths. A fire broke out in Kashiwazaki-Kariwa nuclear power plant from a transformer. Due to the strong shaking exceeding the safety shutdown level, the operation of the power plant has been suspended since then.

Figure 1 shows the study area of this study (Higashi-honmachi), a central part of Kashiwazaki City. Aerial surveys of the city were conducted by three different organizations; Kashiwazaki City Government on 27 April, 2007 (before the earthquake), Asia Air Survey Co., Ltd. and Geographical Survey Institute (GSI), Japan on 19 July, 2007 (two days after the earthquake). The pre-event images of the city government were taken by UltraCam-D digital camera (Leberl and Gruber, 2005) while the post-event images of Asia Air Survey were obtained by DMC digital camera (Hinz, 1999). UltraCam and DMC are the most selling large-format aerial digital cameras in the world. The post-event images by GSI were taken by RC30 analog (film) camera.

Figure 1. Digital aerial image with 12.2 cm resolution for a part of Kashiwazaki City, which was taken two days after the 2007 Mid-Off-Niigata earthquake by Asia Air Survey Co., Ltd.

One of the most advantageous features of aerial digital cameras is that they have a near infrared (NIR) band as well as RGB visible bands. Vegetation is often the cause of changes between two images taken in different seasons. However, using NIR and red (R) bands of digital cameras, vegetation is easily extracted in terms of the normalized vegetation index (NDVI), calculated by

$$NDVI = (NIR - R) / (NIR + R) \quad (1)$$

where R and NIR are the reflectance of the red and near-infrared bands, respectively. NDVI is a simple and reliable index to identify the existence of vegetation, and therefore widely applied to assess the characteristics of the earth surface in the field of satellite remote sensing.

Another important feature of digital aerial images is its high radiometric resolution. Since digital images contain much less noise than scanned-analog photos do, much clear edges can be extracted. Edge extraction is one of the important tools to extract building damage (Mitomi et al., 2002), to estimate the overturning ratio of tombstones due to earthquakes (Nitto and Yamazaki, 2006), and to extract vehicles from aerial images (Liu et al., 2007).

3. PIXEL-BASED SUPERVISED CLASSIFICATION

First, a conventional pixel-based classification was carried out for the post-earthquake digital image (Figure 1) based on the maximum likelihood method, the most common supervised classification method. In the classification, 8 bit values of RGB and NIR bands were used and twelve classes were selected as training data: black roof, white roof, gray roof, red roof, blue roof, road, ground, paved ground, shadow, tree, grass, and debris.

The result of the classification is shown in Figure 2. Vegetation (tree and grass) were correctly classified because the NIR band was used. However, salt-and-pepper noises are seen (Matsumoto et al., 2006) in all the parts of the image. Such noises were generated because the digital aerial image has very-high spatial-resolution which captures fine details, especially in pixel-based classification. Thus, many small

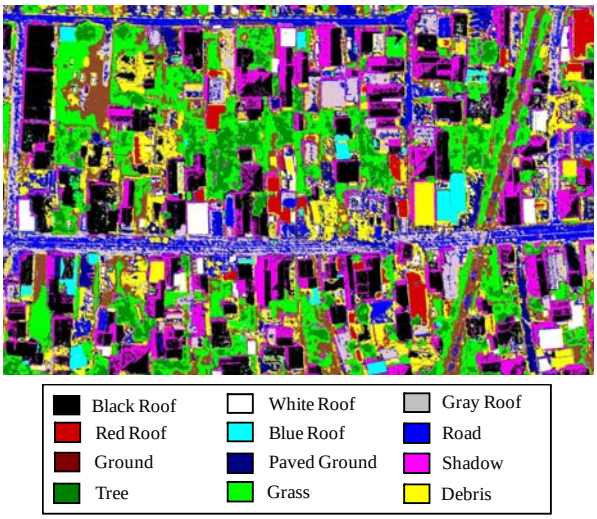

Figure 2. The result of pixel-based supervised classification for the post-event image.

Figure 3. The result of visual extraction of debris.

misclassifications are seen, especially for black-roofs by capturing individual roof-tiles. Another cause of misclassifications is the effect of sunlight. Since sunlight comes from the right side of the image, the brightness of right- and left-side roofs is different.

Figure 3 shows the result of visual extraction of debris for the post-event image. Comparing the debris areas in Figure 2 (yellow) and Figure 3 (red), those by the pixel-based classification look to overestimate the actual debris areas. Debris does not have unique spectral characteristics because it consists of the mixture of woods, mud and roof-tiles. Therefore, a lot of misclassifications as debris were seen in the ground and non-damaged roofs with the color of no training data. Mitomi et al. (2002) introduced a sort of spatial filtering to reduce the salt-and-pepper noise classified as debris. In such approaches, the size of spatial window should be assigned properly, depending on the size of target objects.

4. OBJECT-BASED SEGMENTATION AND SUPERVISED CLASSIFICATION

4.1 Object-based Approach and Segmentation

To solve the salt-and-pepper problem in high-resolution images, object-based classification has recently been introduced. Yamazaki and Kouchi (2006) compared the result from pixel-based classification and that from object-based one for debris detection using QuickBird images in the 2003 Boumerdes, Algeria earthquake. In the study, however, only the post-event image was used and thus, pre-event information, e.g. the location of buildings, was not used effectively. Usefulness of object-based classification is further investigated by Matsumoto et al. (2006) in building damage detection from QuickBird images obtained before and after the 2006 Central Java earthquake. Building areas were extracted for both the pre-event and post-event images by pixel-based and object-based classifications, and their areas were compared. The results showed that the object-based method is suitable to reduce the noise to extract debris from other objects.

In the present study, the digital aerial images with much finer spatial-resolution were employed in performing object-based classification using e-Cognition software (Baatz et al., 2004). Image segmentation was carried out as the first step to make "objects" using the post-event 4 band image. In e-Cognition, the segmentation process is determined by 5 parameters: *Layer Weight*, *Compact Weight*, *Smooth Weight*, *Shape Factor*, and *Scale Parameter*. The most important parameter is *Scale Parameter*, which determines the object size. *Shape Factor* is to determine the importance level of spectral heterogeneity or shape heterogeneity in segmentation. When *Shape Factor* moves toward 0, the spectral heterogeneity is more concerned. On the contrary, if it moves toward 0.9, the shape heterogeneity is more concerned. The spectral heterogeneity is decided by *Layer Weight*, which gives the weight for each spectral band. The shape heterogeneity is decided by *Compact Weight* and *Smooth Weight*; the summation of these values should be 1.0. When *Compact Weight* is larger than *Smooth Weight*, the segmented image objects become a more round shape. On the contrary, when *Smooth Weight* is larger than *Compact Weight*, they become to have smoother borderlines.

Starting from pixels, segmentation runs the merger between two objects and is terminated when an assigned condition is reached. This condition is defined based on the fusion value *f*, which measures the changes when merging. If *f* equals to or becomes bigger than the squared scale parameter, the condition is reached. Although it is difficult to decide the appropriate values of the parameters suitable to all land cover classes, the user can decide the suitable values to a few focused classes, e.g. building, road, and car.

The appropriate parameters for the size of a car was used in this study because the aerial images have very high spatial-resolution and we want to extract debris larger than say, 3-5 m. Considering its resolution (12.2 cm) and the target size of objects (car), *Scale Parameter* was determined as 40 for the post-event image. Figure 4 shows the result of segmentation for the study area and the parameters used. From the figure, objects like cars, roofs, and debris are seen to be segmented properly as one or a few adjacent objects.

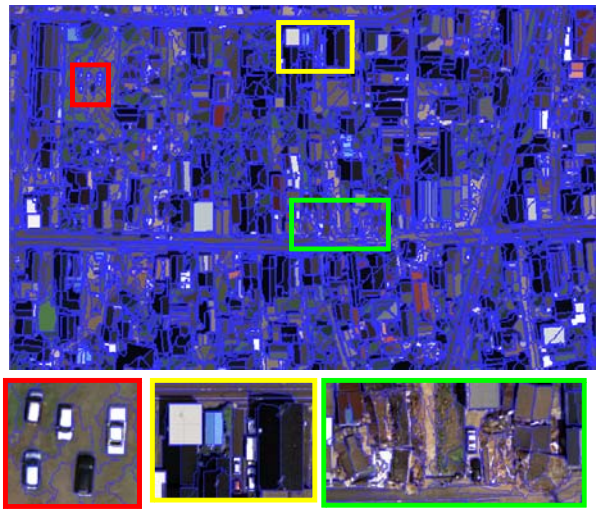

Segmentation parameters
Scale Parameter = 40, *Layer Weight* = 1.0
Shape Factor = 0.5, *Compact Weight* = 0,
Smooth Weight = 1.0

Figure 4. The result of image segmentation for the post-event 4 band image.

4.2 Object-based Supervised Classification

After segmentation, the training areas for all the classes used in the pixel-based classification were assigned as those for the object-based supervised classification. The objects' mean values and standard deviations of 4 spectral bands were used as the indices of classification. In e-Cognition, not only these layer values of image objects but also various feature values of image objects, such as shape, can be considered.

The characteristic object features for debris are with a complex shape and a smaller area than others. In order to extract debris accurately, the object features, that are *Border Length* and *Shape Index*, were employed in the classification.

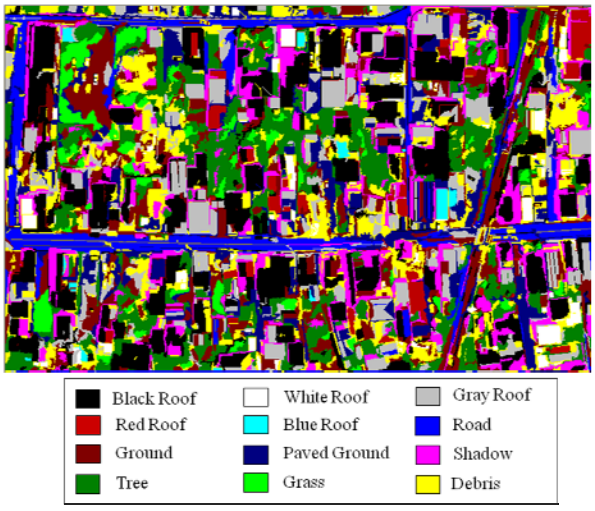

Figure 5. The result of object-based supervised classification for the post-event 4 band image.

The border length is the length of borderline of an image object and the shape index means the degree of complexity of an image object; if an image object has a complex shape, the shape index is given as a high value. The nearest neighbor method was used in a classification step.

The result of the object-based classification for the post-event images is shown in Figure 5. Comparing with the pixel-based classification result (Figure 2), the object-based method looks to classify the images into proper object groups. Salt-and-paper noise is no more seen in case of the object-based classification. Comparing the object-based classification result with the visual inspection result (Figure 3), however, it looks not so satisfactory. The classification result includes a lot of commission errors; some objects like cars, intact roofs, bare grounds, are classified as debris. Since debris contains various materials and possesses various shapes, some objects without proper training areas may be misclassified as debris.

Another drawback of classification methods, both pixel-based and object-based, is necessity to assign many classes and their training data. Actually, if the extraction of debris is the main objective, the classification results for other classes are not so important. If we must extract earthquake damages from many aerial images, the selection of proper classes and training data is time consuming. Thus we will focus only on debris and introduce a level-slice method after the object-based segmentation process.

5. OBJECT-BASED LEVEL-SLICE METHOD FOR DEBRIS EXTRACTION

In order to perform quick damage extraction from digital aerial images, a multi-level slice method is introduced after the object-based segmentation process. Since we focus on the extraction of debris from collapsed houses, color information is not so important. The color of debris is dependent on its material, e.g. roof-tiles, woods, soil, and there is no unique color. Thus a panchromatic image or an intensity (brightness) image is employed instead of RGB color layers. In this study, the intensity (I) is obtained by

$$I = 0.3R + 0.59G + 0.11B \qquad (2)$$

To exclude vegetation, the normalized vegetation index (NDVI) is considered to be another layer value to be used for segmentation and level-slice. For these two layers, segmentation was performed using the same parameter values as Figure 4.

After segmentation, the characteristics of debris objects were investigated in terms of their object features. In this study, the two layer values, *I* and *NDVI*, and five features related to the object shape, *Area*, *Length*, *Width*, *Border Length*, *Average Length of Edges*. To determine the conditions of these object feature values, debris from collapsed houses and roofs of non-damaged houses were used as training areas as shown in Figure 6.

Figure 7 shows the mean and standard deviation of the intensity value for the objects shown in Figure 6. It is observed that the standard deviation for the debris objects is

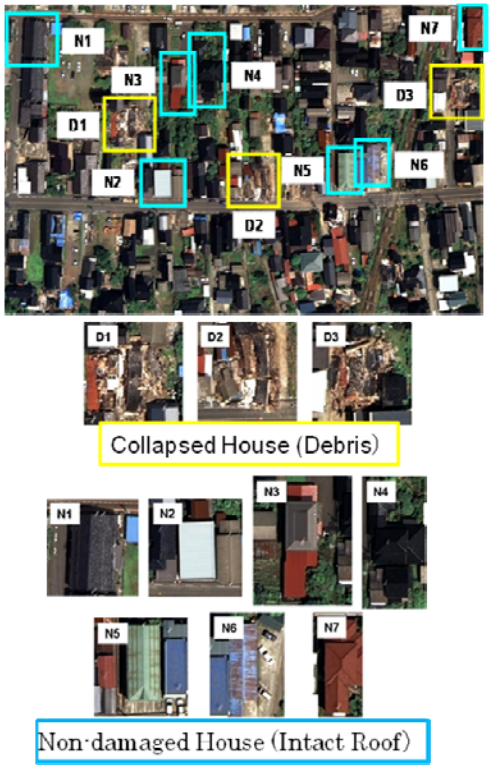

Figure 6. Training areas to determine the condition of object features for debris.

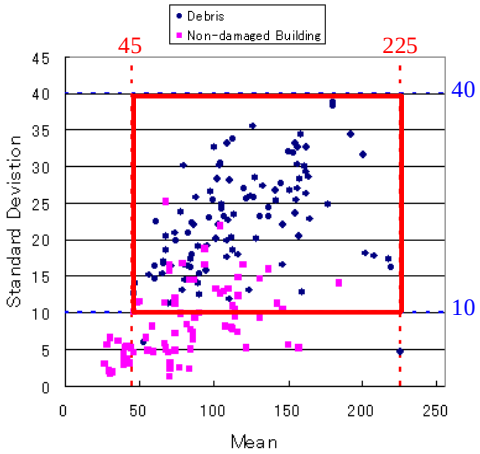

Figure 7. The mean and standard deviation of the intensity of the objects shown in Figure 6. The bounds were used to extract debris objects.

generally bigger than that for the intact roofs. The objects with the mean NDVI value larger than 0.17 were excluded as vegetation in this case. Figure 8 plots the relationship between *Area/Border Length* and *Average Length of Edges* for the training areas. The both values represent irregularity of objects and their conditions to select debris objects are shown in the figure. Figure 9 shows the relationship between *Width* and *Length* for the training areas. To exclude large intact roofs, upper limits were assigned for *Width* and *Length*. Long thin objects, like road lines and shadows, were removed by assigning the threshold of *Length*/*Width*.

The objects satisfying all these conditions were assumed to be considered as debris as shown in Figure 10. Comparing this figure with the visual inspection result, the extracted objects are much more than actual debris. Especially, there are still many small objects which were misclassified as debris. To reduce these commission errors, the pre-event digital image taken by UltraCam-D was employed. The similar debris extraction procedure was applied to this image and the result was shown in Figure 11. Since the debris' threshold values determined for the post-event image were used, many "debris" areas were extracted, as obvious commission errors. The common "debris pixels" in Figures 10 and 11 were removed from Figure 10 to reduce commission errors.

Since there still remain many commission errors, the objects smaller than a minimum area (A_{min}) were further excluded from debris. Figure 12 shows the accuracy of debris extraction with respect to A_{min}. The overall accuracy is considered as the average of producer accuracy and user accuracy. To increase A_{min} value, the user accuracy increases because commission errors (area A in Figure 12) are removed, and the producer accuracy decreases due to reduction of the correctly extracted area (B in Figure 12). The average of the two accuracies gets its maximum value when A_{min} reaches about 58 m^2. But this maximum value does not show a clear peak, a slight change in the extraction procedure may give other A_{min} value.

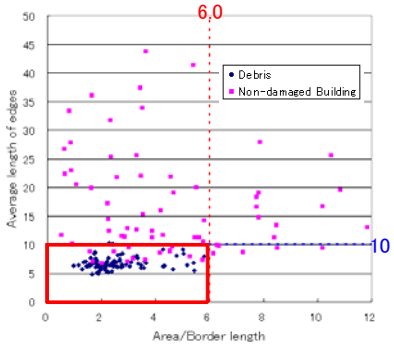

Figure 8. The relationship between *Area/Border Length* and *Average Length of Edges* for the training areas. The bounds were used to extract debris objects.

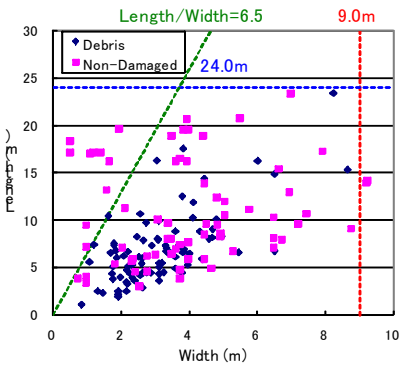

Figure 9. The relationship between *Width* and *Length* for the training areas. The bounds were used to extract debris objects.

Figure 10. The result of extracted debris by the object-based level-slice method. Many small commission errors are seen.

Figure 11. The result obtained by applying the debris extraction procedure to the pre-event digital image.

Figure 13 shows the filtered debris areas at this A_{min} value and the debris areas are in good agreement with the visual inspection result. But this area-filter value is considered to be too large since it is almost the same level as the footprint of an ordinary house in Japan, and hence this kind of area-based accuracy evaluation may have some limitation.

Evaluation of accuracy is further carried out in an object-based manner; if an extracted object has a 50% overlap with an actual debris area, it is counted as correct. Figure 13 shows the accuracy of debris extraction by this object-based counting with respect to A_{min}. The maximum accuracy is obtained when A_{min} reaches about 58 m^2, the

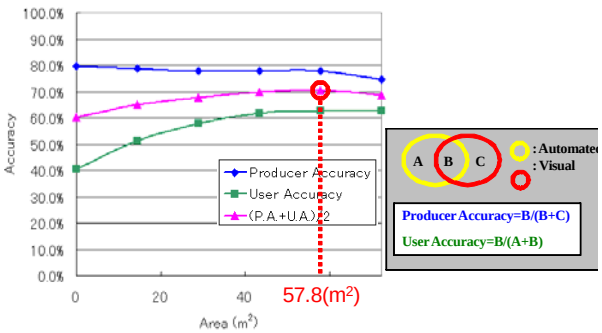

Figure 12. Area-based accuracy of extracted debris by the object-based level-slice method.

Figure 12. The result of extracted debris after subtraction of the pre-event debris areas and applying the minimum area filter (A_{min}=58m^2).

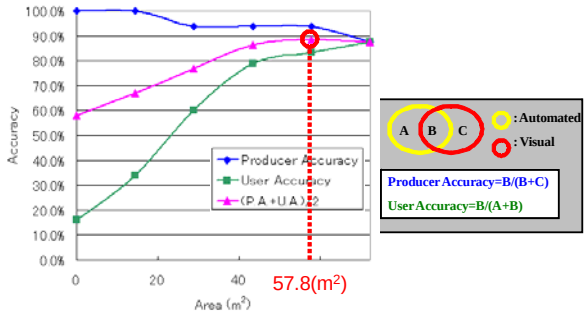

Figure 13. Object-based accuracy of extracted debris by the object-based level-slice method.

same as the area-based accuracy evaluation. However, the peak was much clearer than the previous evaluation. If we try to estimate the number of collapsed houses from aerial images, counting the number of extracted objects by this scheme may give acceptable accuracy. However, the determination of object feature values still need to be tested for many other examples.

6. CONCLUSIONS

Automated building damage extraction was conducted using a digital aerial image captured after the 16 July 2007 Mid-Off-Niigata earthquake. First, a pixel-based maximum likelihood classification was performed. As the result, salt-and-pepper noises and misclassifications were seen. An object-based supervised classification was then performed assigning 12 classes as training data. Although the object-based classification method gives an acceptable level of accuracy, assigning proper classes and training data is time consuming for a large area. Thus a level-slice method was introduced after object-based segmentation. Selecting the intensity and NDVI as layer values and employing several feature values of debris objects, the object-based level-slice method was carried out. The similar debris extraction was also carried out for the pre-event image to remove commission errors in the level-slice debris extraction. Since many small misclassifications were still observed, a minimum area-filter was further applied to remove them. The extracted debris areas show a reasonable level of accuracy, especially in the object-based producer and user accuracy. To enhance the accuracy further, the method should be tested for larger areas and more examples.

Acknowledgements:

The aerial digital image used in this study was provided from Asia Air Survey Co., Ltd and Kashiwazaki City Government.

References:

Baatz, M., Benz, U., et al. (2004). Definiens Imaging, e-Cognition user guide 4, 76-78.

Hinz, A. (1999). The Z/I digital aerial camera system, *Proceedings of the 47th Photogrammetric Week 1999*, Wichmann Verlag, Heidelberg, 109-115.

Leberl, F. and Gruber, M. (2005). ULTRACAM-D: Understanding some Noteworthy Capabilities, *Photogrammetric Week 05*, Dieter Fritsch, Ed. Wichmann Verlag, Heidelberg 57-68.

Liu, W., Yamazaki, F., Vu, T.T., and Maruyama, Y. (2007). Speed Detection of Vehicles from Aerial Photographs, *Proc. 27th Asian Conference on Remote Sensing*, CD-ROM, 6p.

Maruyama, Y., Yamazaki, F., Yogai, H., and Tsuchiya, Y. (2006). Interpretation of Expressway Damages in the 2004 Mid Niigata Earthquake Based on Aerial Photographs, *Proceedings of the First European Conference on Earthquake Engineering and Seismology*, Geneva, Switzerland, CD-ROM, Paper No. 738, 8p.

Matsumoto, K., Vu, T.T., and Yamazaki, F. (2006). Extraction of Damaged Buildings Using High Resolution Satellite Images in the 2006 Central Java Earthquake, *Proc. 27th Asian Conference on Remote Sensing*, CD-ROM, 6p.

Mitomi, H., Matsuoka, M., and Yamazaki, F. (2002). Application of Automated Damage Detection of Buildings due to Earthquakes by Panchromatic Television Images, *The 7th U.S. National Conference on Earthquake Engineering*, CD-ROM, 10p.

Nitto, T. and Yamazaki, F. (2006). Estimation of Overturning Ratio of Tombstones by Image Analysis of Aerial Photographs, *Proc. 27th Asian Conference on Remote Sensing*, CD-ROM, 6p.

Ogawa, N. and Yamazaki, F. (2000). Photo-Interpretation of Building Damage due to Earthquakes using Aerial Photographs, *Proc. 12th World Conference on Earthquake Engineering*, CD-ROM, 8p.

Yamazaki, F., and Kouchi, K. (2006). Automated Damage Detection of Buildings from High-Resolution Satellite Images, *Proceedings of the First European Conference on Earthquake Engineering and Seismology*, Geneva, Switzerland, CD-ROM, Paper No. 714, 7p.